Proceedings of the 28th IEEE
EMBS Annual International Conference
New York City, USA, Aug 30-Sept 3, 2006

Immune Cells Detection of the *In Vivo* Rejecting Heart in USPIO-Enhanced Magnetic Resonance Imaging

Hsun-Hsien Chang and José M. F. Moura
Electrical and Computer Engineering,
Carnegie Mellon University
Pittsburgh, PA 15213, USA
{hsunhsien,moura}@cmu.edu

Yijen L. Wu and Chien Ho*
Department of Biological Sciences and
Pittsburgh NMR Center for Biomedical Research,
Carnegie Mellon University
Pittsburgh, PA 15213, USA

Abstract— **Contrast-enhanced magnetic resonance imaging (MRI) is useful to study the infiltration of immune cells, in particular macrophages. Contrast agents, for example ultrasmall superparamagnetic iron oxide (USPIO) particles, administered intravenously into the blood stream will be engulfed by macrophages circulating in the circulation system. When a transplanted heart rejects, macrophages and other immune cells will infiltrate the rejecting tissue. Imaged by T_2^* weighted MRI, USPIO-labeled macrophages will display dark pixel intensities. Detecting the presence of USPIO particles in the images facilitates the study of heart rejection.**

We cast the problem of detecting the presence of USPIO-labeled myocardium in the framework of spectral graph theory, and treat our decision function as a level set function on the image. The pixels with positive level set values correspond to the presence of immune cells, and negative to the absence. When the image is modeled by a graph, the spectral analysis of the graph Laplacian provides a basis to represent the level set function. We develop from the Cheeger constant of the graph an objective functional of the level set function. The minimization of the objective leads to the optimal level set function. Experimental results suggest the feasibility of our approach in the study of rejecting hearts.

I. Introduction

Contrast-enhanced magnetic resonance imaging (MRI) is a useful tool to monitor the role of immune cells in many pathophysiological processes. In 1990, Weissleder *et al.* [1] introduced a new contrast agent, ultrasmall superparamagnetic iron oxide (USPIO), which has superior relaxivity due to its magnetite core and whose size is about only 20nm. Physicians have adopted USPIO-enhanced imaging to monitor the infiltration of immune cells in organ dysfunction, such as neural disorder [2], myocardial infarction [3], heart rejection [4], and renal disease [5].

After dextran-coated USPIO particles are administered intravenously into the circulation system, immune cells, mainly macrophages, will ingest the particles. Hence, macrophages make themselves *USPIO-labeled*. When heart rejection occurs, macrophages migrate to the rejecting tissue. Under T_2^* weighted MRI, the USPIO particles display dark pixels that precisely localize the rejection [4], [6]. For example, Figure 3(a) shows the left ventricular images of two rejecting hearts, where the darker intensities in the epicardium reveal the presence of USPIO particles, leading to an understanding of where the macrophages accumulate. To identify the accumulation regions, the first task is to detect the USPIO-labeled areas. However, the challenges to detect the USPIO particles are twofold:

1) Macrophages accumulate in multiple regions without known patterns, so cardiologists must scrutinize the entire image to determine dark pixels.
2) The heart motion blurs the image, so it is very difficult to correctly decide where the dark pixels are.

Such manual detection process is labor-intensive and time-consuming, and the results are operator dependent. To reduce the labor work and to achieve consistent detection, we need an automatic algorithm to detect USPIO-labeled pixels.

We treat our decision function as a level set function on the image. The pixels with positive level set values are determined as USPIO-labeled. In the framework of spectral graph theory [7], the eigenfunctions of the graph Laplacian span the Hilbert space of the square integrable functions defined on the vertices of the graph. To utilize this fact, we model the image by a graph. Then, eigendecomposing the Laplacian of the graph provides basis functions whose linear combination represents our desired level set function. We derive from the Cheeger constant of the graph an objective functional of the level set function. Minimization of the objective functional determines the optimal level set function. Masking out the positive level set function finds out the USPIO-labeled pixels.

The organization of this paper is as follows. Section II develops our algorithm in the framework of spectral graph theory. In Section III, we describe the algorithm implementations and show our experimental results for USPIO-enhanced images. Finally, Section IV concludes this paper.

II. Methodology

For a given image, we want to find out a level set function g on the image domain Ω. We arrange all the pixels into a single column vector, and then the level set function is denoted by vector $\mathbf{g}$. The pixels which have positive level set consist of the desired USPIO-labeled regions. If there are basis functions $\{\phi^{(j)}\}$ on the image, we can express the level set function $\mathbf{g}$ as a linear combination of the basis; that is,

$$\mathbf{g} = \sum_j a_j \phi^{(j)} \,. \tag{1}$$

*This work was supported by NIH grants, R01EB/AI-00318 and P41EB001977, to the Pittsburgh NMR Center for Biomedical Research, Carnegie Mellon University.

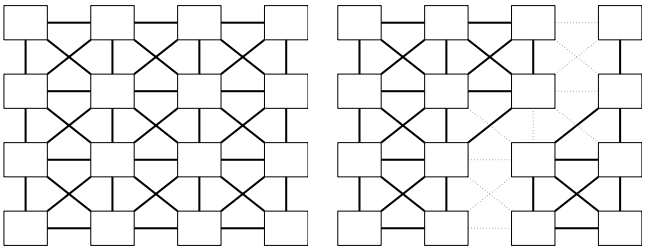

(a) Image pixels are connected to their neighborhoods. (b) Dotted edges assemble an edge cut of the graph.

Fig. 1. Graph representation of a 4×4 image.

We use the framework of spectral graph theory to obtain the basis, described in Section II-A. To find the optimal level set function $\mathbf{g}$, we develop an objective functional $Q(\mathbf{g})$ in Section II-B that is derived from the Cheeger constant of the graph. After obtaining the basis functions $\phi^{(j)}$, looking for the optimal level set function $\mathbf{g}$ by minimization of $Q(\mathbf{g})$ is equivalent to finding the optimal coefficients a_j. In Section II-C, we reformulate the objective functional in terms of the coefficients a_j, and derive the equations needed to obtain the optimal a_j.

A. Basis Functions

We represent the image by a graph $G(V, E)$. Figure 1(a) illustrates the graph representation of a 4×4 image, where each square is a pixel. The vertex set V of the graph G is a set of N, say 16 in Figure 1(a), vertices denoting all the pixels in the image. The edge set E of the graph G consists of edges e_{ij} linking the vertices v_i and v_j. For a vertex v_i, we assign edges e_{ij} connecting it to the neighboring eight vertices v_j.

Associated with the graph G, we have the weighted adjacency matrix $\mathbf{W}$ whose entries W_{ij} are given below:

$$W_{ij} = \begin{cases} \exp\left(-\frac{\|f_i - f_j\|^2}{\sigma^2}\right), & \text{if there is the edge } e_{ij} \\ 0, & \text{if no edge } e_{ij} \end{cases}, \tag{2}$$

where f_i is the intensity of the pixel i. The degree d_i of the vertex v_i is the weighted sum of the edges connecting to itself, or equivalently

$$d_i = \sum_j W_{ij} \,. \tag{3}$$

The Laplacian $\mathbf{L}$ of the graph is defined as, see [7],

$$\mathbf{L} = \mathbf{D} - \mathbf{W} \tag{4}$$

where $\mathbf{D} = \text{diag}\,(d_1, d_2, \cdots, d_N)$ is a diagonal matrix of vertex degrees. Spectral analysis of the graph Laplacian $\mathbf{L}$ gives the eigenvalues $\{\lambda_j\}_{j=0}^{N-1}$ and eigenfunctions $\{\phi^{(j)}\}_{j=0}^{N-1}$. By convention, we index the eigenvalues in ascending order.

In the framework of spectral graph theory [7], the eigenfunctions $\{\phi^{(j)}\}$ form a basis of the Hilbert space of square integrable functions on the vertices. The eigenfunctions with small eigenvalues correspond to the low frequency harmonics. Linearly combining the first p eigenfunctions can represent a *smooth* level set function $\mathbf{g}$; i.e.,

$$\mathbf{g} = \sum_{j=1}^{p} a_j \phi^{(j)} = \Phi \mathbf{a} \,, \tag{5}$$

where $\Phi = \left[\phi^{(1)}, \phi^{(2)}, \cdots, \phi^{(p)}\right]$. In the sequel, the problem of looking for the optimal level set function becomes the one of finding the optimal linear combination coefficient vector $\mathbf{a}$.

B. Cheeger Constant

We can think of the zero level set as an *edge cut* in the graph G. An edge cut is a subset E_0 of edges whose removal disjoins the graph G into two subgraphs $G_1 = (V_1, E_1)$ and $G_2 = (V_2, E_2)$; note that $V = V_1 \cup V_2$, $\emptyset = V_1 \cap V_2$, $E = E_0 \cup E_1 \cup E_2$, and $\emptyset = E_1 \cap E_2$. With reference to the example in Figure 1(b), the dotted edges assemble an edge cut; removing this edge cut partitions the graph. Spectral graph theory [7] shows that solving the edge cut is equivalent to determining the Cheeger constant

$$C(V_1) = \min_{V_1} \frac{|E_0(V_1)|}{\text{vol}(V_1)} \,, \tag{6}$$

assuming that $\text{vol}(V_1) \leq \text{vol}(V_2)$ is fixed. In equation (6), $|E_0(V_1)|$ is the sum of the edge weights in the cut E_0:

$$|E_0(V_1)| = \sum_{e_{ij} \in E_0} W_{ij} \,, \tag{7}$$

and $\text{vol}(V_1)$ is the volume of V_1 defined as the sum of the vertex degrees in the V_1:

$$\text{vol}(V_1) = \sum_{v_i \in V_1} d_i \,. \tag{8}$$

When we define a function $\mathbf{y}$ on the graph as

$$y_i = \begin{cases} 1, & \text{if } v_i \in V_1 \\ 0, & \text{if } v_i \in V_2 \end{cases}, \tag{9}$$

the Cheeger constant is

$$C(\mathbf{y}) = \min_{\mathbf{y}} \frac{\mathbf{y}^T \mathbf{L} \mathbf{y}}{\mathbf{y}^T \mathbf{d}} \,. \tag{10}$$

To obtain the optimal $\mathbf{y}$ is equivalent to minimizing an objective functionial

$$Q(\mathbf{y}) = \mathbf{y}^T \mathbf{L} \mathbf{y} - \beta \mathbf{y}^T \mathbf{d} \,, \tag{11}$$

where β is the weight.

C. Optimal Coefficients a_j for the Level Set Function

We can relate the objective functional Q in equation (11) to the level set function (5). Assume that the vertices with level set greater than zero belong to V_1. Using the standard Heaviside function

$$\mathcal{H}(g) = \begin{cases} 1, & \text{if } g \geq 0 \\ 0, & \text{if } g < 0 \end{cases}, \tag{12}$$

we can mask out the vertex set V_1. To facilitate numerical implementation, the regularized Heaviside function $h(g)$ and

its derivative, the regularized delta function $\delta(g)$, are often used; they are defined, respectively, as

$$h(g) = \frac{1}{2}\left[1 + \frac{2}{\pi}\arctan\left(\frac{g}{\epsilon}\right)\right], \tag{13}$$

and

$$\delta(g) = \frac{dh(g)}{dg} = \frac{1}{\pi}\left(\frac{\epsilon}{\epsilon^2 + g^2}\right). \tag{14}$$

Replacing $\mathbf{y}$ in equation (11) with the Heaviside function on the level set, we obtain the objective functional

$$Q(\mathbf{g}) = \mathbf{h}(\mathbf{g})^T \mathbf{L}\mathbf{h}(\mathbf{g}) - \beta \mathbf{h}(\mathbf{g})^T \mathbf{d}\,. \tag{15}$$

Since the level set function $\mathbf{g}$ is parametrized by the coefficient vector $\mathbf{a}$, the argument of the objective functional Q is this vector $\mathbf{a}$, i.e.,

$$Q(\mathbf{a}) = \mathbf{h}(\mathbf{g}(\mathbf{a}))^T \mathbf{L}\mathbf{h}(\mathbf{g}(\mathbf{a})) - \beta \mathbf{h}(\mathbf{g}(\mathbf{a}))^T \mathbf{d}\,. \tag{16}$$

Minimizing Q with respect to $\mathbf{a}$ gives the optimal coefficient vector $\hat{\mathbf{a}}$ for the level set function $\mathbf{g}$.

Taking the gradient of $Q(\mathbf{a})$ leads to

$$\frac{\partial Q}{\partial \mathbf{a}} = 2\left(\frac{\partial \mathbf{h}^T}{\partial \mathbf{a}}\right)\mathbf{L}\mathbf{h} - \beta\left(\frac{\partial \mathbf{h}^T}{\partial \mathbf{a}}\right)\mathbf{d}\,. \tag{17}$$

In equation (17), the computation of $\left(\frac{\partial \mathbf{h}^T}{\partial \mathbf{a}}\right)$ is

$$\left(\frac{\partial \mathbf{h}^T}{\partial \mathbf{a}}\right) = \left[\frac{\partial h_1}{\partial \mathbf{a}}, \frac{\partial h_2}{\partial \mathbf{a}}, \cdots, \frac{\partial h_N}{\partial \mathbf{a}}\right] \tag{18}$$

$$= \begin{bmatrix} \frac{\partial h_1}{\partial a_1} & \frac{\partial h_2}{\partial a_1} & \cdots & \frac{\partial h_N}{\partial a_1} \\ \vdots & \vdots & \cdots & \vdots \\ \frac{\partial h_1}{\partial a_p} & \frac{\partial h_2}{\partial a_p} & \cdots & \frac{\partial h_N}{\partial a_p} \end{bmatrix}. \tag{19}$$

Using the chain rule, the entries $\left(\frac{\partial \mathbf{h}^T}{\partial \mathbf{a}}\right)_{mn}$ are

$$\left(\frac{\partial \mathbf{h}^T}{\partial \mathbf{a}}\right)_{mn} = \frac{\partial h_n}{\partial a_m} = \frac{\partial h_n}{\partial g_n}\frac{\partial g_n}{\partial a_m} \tag{20}$$

$$= \delta(g_n)\frac{\partial \sum_j a_j \phi_n^{(j)}}{\partial a_m} \tag{21}$$

$$= \delta(g_n)\phi_n^{(m)}\,. \tag{22}$$

Written explicitly, $\left(\frac{\partial \mathbf{h}^T}{\partial \mathbf{a}}\right)$ is

$$\left(\frac{\partial \mathbf{h}^T}{\partial \mathbf{a}}\right) = \begin{bmatrix} \delta(g_1)\phi_1^{(1)} & \delta(g_2)\phi_2^{(1)} & \cdots & \delta(g_N)\phi_N^{(1)} \\ \vdots & \vdots & \cdots & \vdots \\ \delta(g_1)\phi_1^{(p)} & \delta(g_2)\phi_2^{(p)} & \cdots & \delta(g_N)\phi_N^{(p)} \end{bmatrix}$$

$$= \Phi^T \Delta\,, \tag{23}$$

where we define Δ as a diagonal matrix:

$$\Delta = \mathrm{diag}\left(\delta(g_1), \delta(g_2), \cdots, \delta(g_N)\right). \tag{24}$$

Substituting (23) into (17), the gradient of the objective has a compact form

$$\frac{\partial Q}{\partial \mathbf{a}} = 2\Phi^T \Delta \mathbf{L}\mathbf{h} - \beta \Phi^T \Delta \mathbf{d}\,. \tag{25}$$

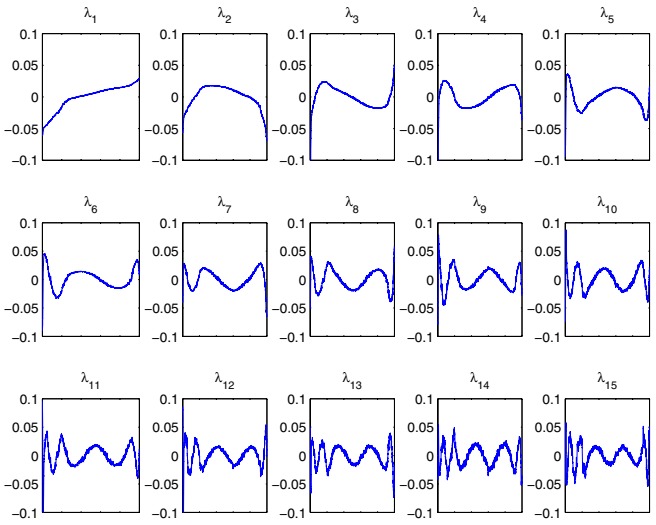

Fig. 2. The first 15 eigenfunctions used to represent the level set function.

To obtain the optimal coefficient vector $\hat{\mathbf{a}}$, we have to solve the minimization numerically, because $\mathbf{a}$ is embedded in the matrix Δ and in the vector $\mathbf{h}$ in equation (25). We adopt the gradient descent algorithm to iteratively find the solution $\hat{\mathbf{a}}$ making $\frac{\partial Q}{\partial \mathbf{a}} = 0$. After obtaining $\hat{\mathbf{a}}$, the level set function $\mathbf{g}$ is determined by

$$\mathbf{g} = \Phi\hat{\mathbf{a}}\,. \tag{26}$$

Making out the pixels with positive level set values produces our desired regions with macrophage accumulation.

III. Experiments

This section presents experimental results. We consider the algorithm and then show the results on USPIO-enhanced heart images.

Algorithm: We implement our algorithm with MATLAB® on a computer with a 2.6 GHz CPU and 512 MB RAM. To derive the image graph, we set $\sigma^2 = 0.01$ when computing the edge weights in (2). The parameter ϵ for the regularized Heaviside and delta functions in (13) and (14), respectively, is set to 0.1. We choose the first 15 eigenfunctions of the graph Laplacian to represent our level set function. Figure 2 shows these eigenfunctions. The lower order eigenfunctions are smoother basis harmonics, so their linear combination leads to a smooth level set function.

To implement the minimization step, we first need to determine the parameter β in the objective functional (16). One important observation is that the first term in (16) is significantly smaller than the second term. If β is not small enough, the second term dominates and the level set function reduces to a positive constant, leading to every pixel being detected as USPIO-labeled. To strike a balance between the two terms, we empirically determine $\beta = 0.05$. To reach the minimum of the objective functional, we solve $\frac{\partial Q}{\partial \mathbf{a}} = 0$ recursively. We stop the iterative process when the norm of

the gradient is smaller than 10^{-4} or when the minimization reaches 100 iterations.

Application to USPIO-enhanced MR Images of Rejecting Heart Transplants: We study the rejection of transplanted hearts on rats. All rats are male inbred Brown Norway (BN) or Dark Agouti (DA), with body weight between $180 - 230$ grams each, obtained from Harlan (Indianapolis, IN). We transplant DA hearts to BN hosts. Dextran-coated USPIO particles [6] of 27nm in size are administered intravenously one day prior to MRI with the dosage of 4.5 milligrams per kilogram bodyweight. *In vivo* imaging is carried out on a Bruker AVANCE DRX 4.7 Tesla system. All the scans are transversal slices near the equator of the left ventricles.

After data acquisition, we manually segment out the left ventricle. For example, the images in Figure 3(a) show different transplanted hearts at end-diastole imaged on post-operation days (POD) 3 and 4. Then, we apply our detection algorithm to the images. Figure 3(b) show the detected USPIO-labeled pixels denoted by red dots. Unlike time-consuming manual detection, our algorithm determines the regional macrophage accumulation within two minutes for each image.

To evaluate the performance of our algorithm, we treat the manual detection as the ground truth. Two of the authors (Chang and Wu) manually labeled the macrophage pixels, shown in Figure 3(c), before running the automatic algorithm. Our automatically detected regions show high agreement with the manual detection results. This validation suggests that our approach is useful in the study of heart rejection based on the USPIO-enhanced MRI data.

From the detected results shown in Figure 3(b), we see that the rejecting hearts have heterogeneous patterns of macrophage infiltration. The biological reason for the heterogeneity is under investigation. In the future work, we will adopt MR tagging to monitor the motion of the heart transplants and will investigate the histopathology of the transplants.

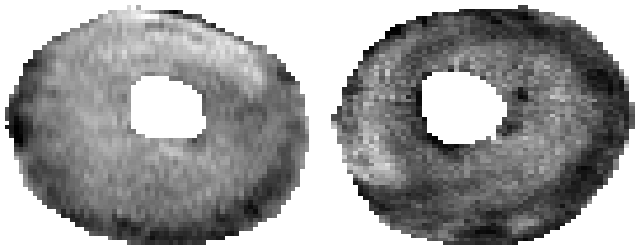

(a) USPIO-enhanced images.

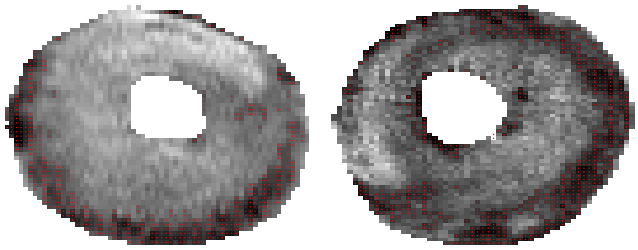

(b) Automatically detected results.

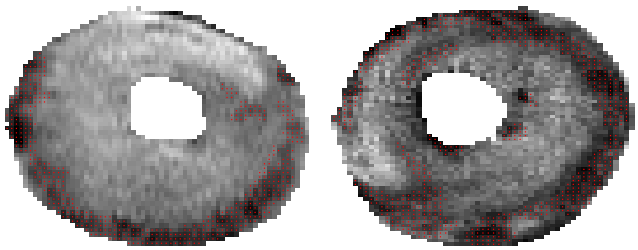

(c) Manually detected results.

Fig. 3. Application of our algorithm to rejecting heart transplants. Red dots label detected pixels with macrophage accumulation. Left: POD3. Right: POD4.

IV. Conclusions

In this paper, we develop an automatic algorithm to detect regional macrophage accumulation of transplanted hearts imaged by USPIO-enhanced MRI. We treat the decision function as a level set function with positive values on the USPIO-labeled pixels. We model an image by a graph with vertices denoting pixels and edges connecting neighboring pixels. The eigendecomposition of the graph Laplacian provides a basis to represent the smooth level set function. The optimal level set function is achieved by minimizing an objective functional derived from the Cheeger constant of the graph. The experimental results show that the detector developed in this paper can determine accurately the regional infiltration of immune cells and can assist the study of rejecting heart transplants.

References

[1] R. Weissleder, G. Elizondo, J. Wittenberg, C. A. Rabito, H. H. Bengele, and L. Josephson, "Ultrasmall superparamagnetic iron oxide: Characterization of a new class of contrast agents for MR imaging," *Radiology*, vol. 175, pp. 489–493, 1990.

[2] J. W. M. Bulte, S.-C. Zhang, P. van Gelderen, V. Herynek, E. K. Jordana, I. D. Duncan, and J. A. Frank, "Neurotransplantation of magnetically labeled oligodendrocyte progenitors: Magnetic resonance tracking of cell migration and myelination," *Proceedings of the National Academy of Sciences of the United States of America*, vol. 96, no. 26, pp. 15256–15261, 1999.

[3] L. J. M. Kroft, J. Doornbos, R. J. van der Geest, A. van der Laarse, H. van der Meulen, and A. de Roos, "Ultrasmall superparamagnetic particles of iron oxide (USPIO) MR imaging of infarcted myocardium in pigs," *Magnetic Resonance Imaging*, vol. 16, no. 7, pp. 755–763, October 1998.

[4] Y. L. Wu, Q. Ye, L. M. Foley, T. K. Hitchens, K. Sato, J. B. Williams, and C. Ho, "*In situ* labeling of immune cells with iron oxide particles: An approach to detect organ rejection by cellular MRI," *Proceedings of the National Academy of Sciences of the United States of America*, vol. 103, no. 6, pp. 1852–1857, February 2006.

[5] Y. Sun, D. Yang, Q. Ye, M. Williams, J. M. F. Moura, F. Boada, Z.-P. Liang, and C. Ho, "Improving spatiotemporal resolution of USPIO-enhanced dynamic imaging of rat kidneys," *Magnetic Resonance Imaging*, vol. 21, pp. 593–598, 2003.

[6] S. Kanno, Y. L. Wu, P. C. Lee, S. J. Dodd, M. Williams, B. P. Griffith, and C. Ho, "Macrophage accumulation associated with rat cardiac allograft rejection detected by magnetic resonance imaging with ultrasmall superparamagnetic iron oxide particles," *Circulation*, vol. 104, pp. 934–938, 2001.

[7] F. R. K. Chung, *Spectral Graph Theory*, vol. 92 of *CBMS Regional Conference Series in Mathematics*, American Mathematical Society, 1997.